MATERIALS SCIENCE

Pneumatic cells toward absolute Gaussian morphing

Tian Gao, José Bico, Benoît Roman*

On a flat map of the Earth, continents are inevitably distorted. Reciprocally, curving a plate simultaneously in two directions requires a modification of in-plane distances, as Gauss stated in his seminal theorem. Although emerging architectured materials with programmed in-plane distortions are capable of such shape morphing, an additional control of local bending is required to precisely set the final shape of the resulting three-dimensional surface. Inspired by bulliform cells in leaves of monocotyledon plants, we show how the internal structure of flat panels can be designed to program bending and in-plane distortions simultaneously when pressurized, leading to a targeted shell shape. These surfaces with controlled stiffness and fast actuation are manufactured using consumer-grade materials and open a route to large-scale shape-morphing robotics applications.

Plants leaves and petals provide a good example of shape morphing induced by differential growth and are a source of inspiration for engineering (*1*). Materials capable of changing shape find numerous applications ranging from the fabrication of complex microstructures (*2*) and the manipulation of fragile objects (*3*, *4*) or soft-robotics devices (*5*–*8*) to locomotion in complex environments (*9*) or the design of deployable shelters (*10*). Although basic grabbing devices rely on bending linear beams through bilayer effects (*11*), shape morphing of surfaces poses a much greater geometrical challenge. If distances along the plane of a surface (i.e., the metrics) are conserved, then its Gaussian curvature (i.e., the product of its two principal curvatures) is strictly conserved, restricting the achievable shapes to families of isometries (e.g., cylinders or cones for a sheet of paper). General morphing of a surface, such as when a plane takes on a doubly curved shape, referred to here as Gaussian morphing, requires metric distortion (*12*). In natural structures, such metric changes result from differential growth (*13*, *14*). Engineered systems rely on equivalent nonhomogeneous transformations such as swelling of hydrogels (*15*–*18*), relaxation of liquid crystal elastomers (*19*) or prestretched polymeric filaments (*20*, *21*), inflatable structures (*22*–*24*), and origami or kirigami tesselation (*25*–*27*). Although the shape of a surface is rigorously defined by both curvature and metric tensors, these two parameters are generally not addressed simultaneously except for a few elegant exceptions involving very compliant materials relying on relatively slow swelling actuation (*28*–*30*). Programming complete morphing in stiff structures with fast actuation that are relevant for engineering applications remains a challenge.

Laboratoire de Physique et Mécanique des Milieux Hétérogènes (PMMH), CNRS, ESPCI Paris, Université PSL, Sorbonne Université, Université Paris Cité, 75005 Paris, France.
*Corresponding author. Email: benoit.roman@espci.fr.

In the realm of botany, the leaves of monocotyledon plants such as corn are able to curl inward reversibly under dry conditions, limiting evaporation (Fig. 1A). Actuation relies on peculiar bulliform cells that change their volume depending on turgor pressure (*31*, *32*), producing in-plane extension or contraction of one side of the surface leaf. Inspired by this example from nature, we designed thin panels embedded with inflatable cells referred to as pneumatic Gaussian cells. Both in-plane contraction and angular deflection of the panels can be programmed simultaneously through the cell's design, leading to stiff, three-dimensional (3D) structures. This qualitative step constitutes an important milestone toward versatile morphing robotics applications.

Contracting and bending simultaneously

The elementary unit of a Gaussian cell is based on trapezoidal channels 3D printed on a layer of airtight fabric (Fig. 1B). A heat-sealed layer of the same fabric closes the cell (for the detailed fabrication process, see the supplementary materials and movie S1). The different channels embedded in the thin sandwich are connected to a pressure source. Pneumatic actuation of the cells induces the transformation of the initially flat panel into a complex shape such as a curve-folded origami structure (Fig. 1C and movie S1). Figure 2A presents the deployment

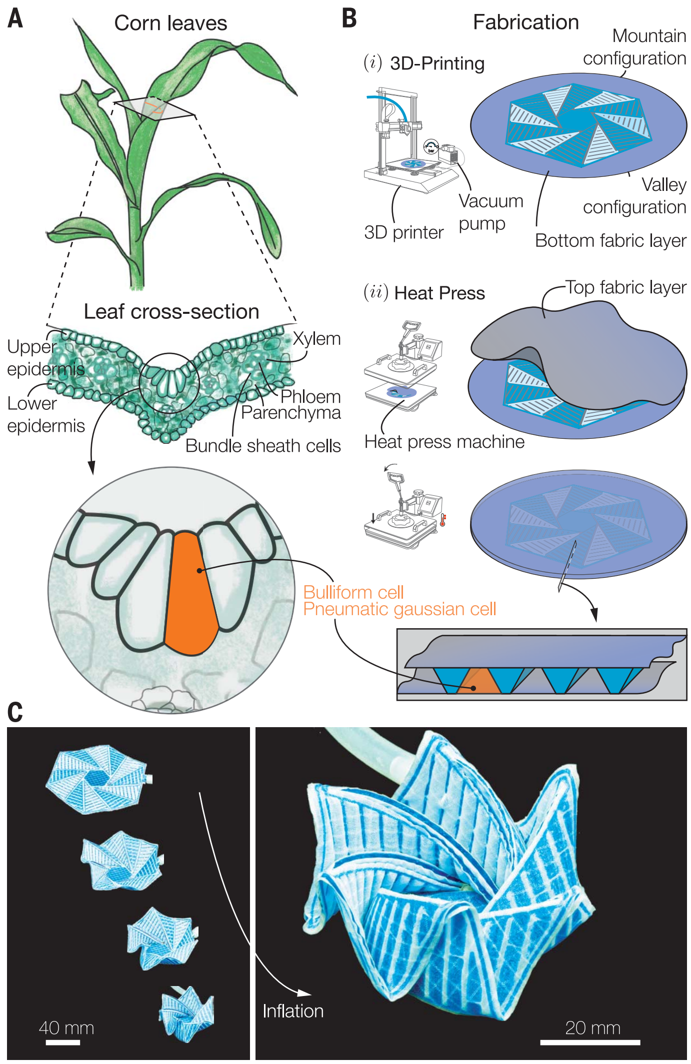

Fig. 1. Production of pneumatic Gaussian cells inspired by leaf bulliform cells. (**A**) Leaves of corn open or close as a function of weather conditions by inflating of deflating bulliform cells under turgor pressure. (**B**) Fabrication of a shape-morphing structure based on pneumatic Gaussian cells. (i) Tilted thermoplastic polyurethane (TPU) walls are 3D printed over a first layer of TPU-coated fabric. (ii) Gaussian cells (orange) are formed by sealing a second layer of fabric on the top of the structure with a heating press. (**C**) Upon inflation (see movie S1), an initially flat panel composed of programmed Gaussian cells self-shapes into a complex 3D structure inspired by the starshade project (*42*, *43*).

mechanism of a plate composed of juxtaposed parallel Gaussian cells with spacial periodicity ℓ. Because the base and the top of the cells are sealed with highly bendable but inextensible fabric, the cells tend to bulge into circular arcs upon inflation, inducing an inward displacement and rotation of the lateral walls. The general case of a symmetric trapezoidal cross-section (orange cells in Fig. 2A) is characterized by the thickness of the plate H, the shortest width W, and the internal angle β of the cell walls (see the supplementary materials for the case of asymmetric cells). The inflated shape of a Gaussian cell is readily obtained from energy minimization (for details, see the supplementary materials). The resulting folding angle γ of the cell is a solution of

$$\begin{aligned}&\left(\beta - \frac{\gamma}{2}\right)\\ &\quad = \sin\beta \cos\left[\left(\beta - \frac{\gamma}{2}\right)\left(\frac{W}{H}\cot\beta + 1\right)\right] \qquad (1)\end{aligned}$$

Inflation also reduces the length of the mid-segment of the cell by a factor λ (Fig. 2B). This quantity referred to as in-plane contraction is solution of

$$\begin{aligned}\lambda = \frac{\cos\left(\beta - \frac{\gamma}{2}\right)}{\left(\beta - \frac{\gamma}{2}\right)\cos\frac{\gamma}{2}} \sin\left[\left(\beta - \frac{\gamma}{2}\right)\left(\frac{W}{H}\cot\beta + 1\right)\right]\\ \left(\frac{W}{H}\cot\beta + 1\right) \qquad (2)\end{aligned}$$

The two extreme cases highlighted in yellow and green in Fig. 2 correspond to cells of rectangular ($\beta = 0°$) and triangular ($W/H = 0$) cross-sections that only provide in-plane contraction or deflection, respectively. Experimental values of γ and λ obtained over a wide range of geometrical parameters show excellent agreement (Fig. 2, B and C) with theoretical predictions (Eqs. 1 and 2). Figure 2, C and D, presents the wide palette of contraction ratio and folding angle as a function of the geometry of inflatable cells parameterized by their internal angle β and aspect ratio W/H. Large folding angles are found in the upper part of the parameter space, whereas large internal angles β promote asymmetry across the thickness of the cell, and values as large as $\gamma > 90°$ can be obtained. The largest contraction is intuitively obtained in the lower right corner, for large W/H. Contraction ratio and folding angle vary along different patterns in the parameter space. For instance, point (ii) in Fig. 2, D and E, corresponds to the same contraction as point (i) but to a larger folding angle. An important consequence is that arbitrary combinations of (λ,γ) can be programmed.

Stiff pneumatic Gaussian cells

Gaussian morphing requires large in-plane deformations and is therefore usually associated with low stiffness (*15*, *17*, *19*, *28*). Pneumatic

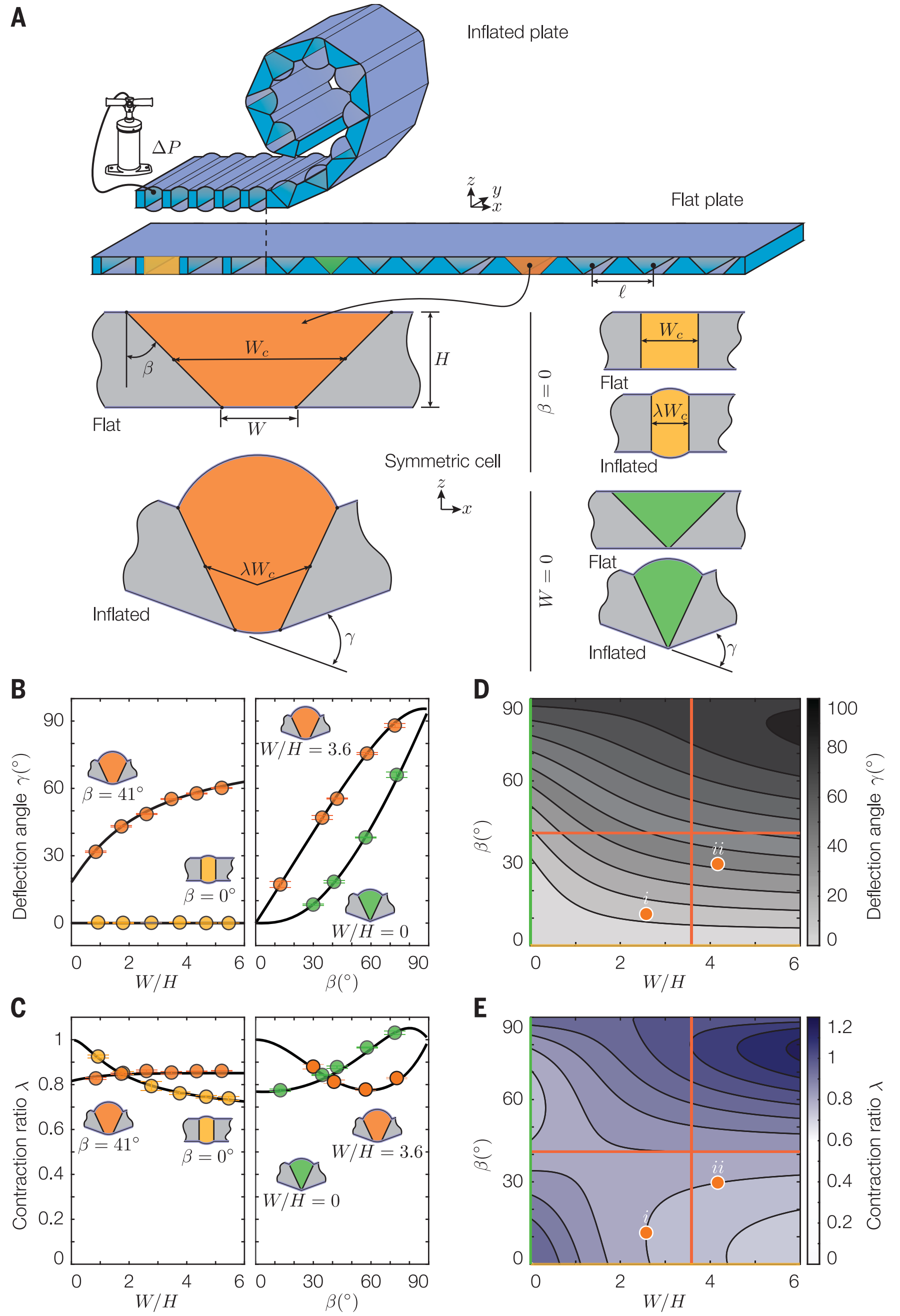

Fig. 2. Programming deformation of Gaussian cells. (**A**) Schematic illustration of the deployment of a flat plate based on three types of symmetric cells. Shown is a generic trapezoidal cell (orange) with walls of thickness H tilted by an angle β and separated by a distance W. Upon inflation, the cell induces a local deflection γ and a contraction λ with respect to the median line W_c. Rectangular cell (yellow) and triangular cell (green) configurations correspond to vertical walls ($\beta = 0$) or to contacting bases ($W = 0$), respectively. (**B** and **C**) Deflection angle γ and contraction ratio λ as a function of the dimensionless width W/H and of the tilt angle β for fixed values of β or W/H, respectively. Solid black lines correspond to theoretical predictions (Eqs. 1 and 2). (**D** and **E**) Landscape of programmable deformations. Shown are theoretical contour maps of the contraction ratio λ and deployed angle γ in a general configuration.

Gaussian cells provide substantial load-bearing capabilities, which can be adjusted not only by pressure but also by the geometry of the cell, a feature distinct from traditional inflatable structures. Their stretching stiffness is assessed by testing the mechanical response of a symmetric cell ($\beta = 0°$) loaded in the direction perpendicular to the channel walls (Fig. 3A). Figure 3B shows the tension force F as a function of the net displacement Δ for a given

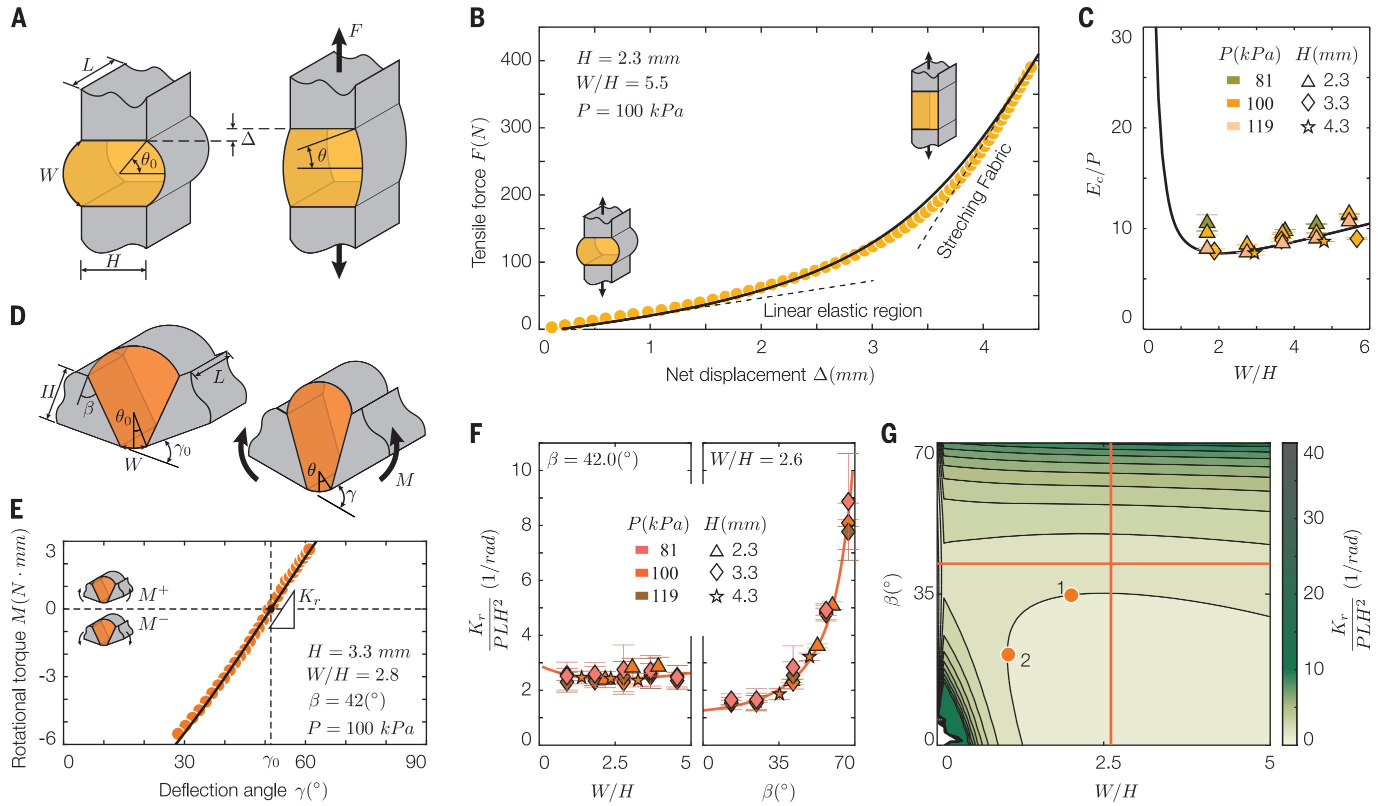

Fig. 3. Mechanical properties of an inflated cell. (**A** to **C**) Stretching modulus. (A) Inflated rectangular cell at rest and under tension with span angle θ and net displacement Δ. (B) Force-displacement curve of an inflated rectangular cell of height H = 2.3 mm and dimensionless width W/H = 5.5 under a pressure P = 10.0 kPa (solid yellow circles). Solid black line indicates theoretical predictions. (C) Dimensionless stretching modulus E_c/P as a function of dimensionless width W/H for various pressures and different cell heights. Solid black line indicates a comparison with the theoretical predictions from Eq. 3. (**D** to **G**) Bending stiffness. (D) Bending test of of an inflated trapezoidal cell. (E) Starting from an equilibrium deflection angle γ_0, applying a torque M results in a new angle γ (H = 3.3 mm, W/H = 2.78, β = 41.5°, P = 10.0 kPa). The slope of the curve in the vicinity of γ_0 = 50.8° corresponds to the rotational stiffness K_r. (F) Rescaled rotational stiffness K_r/PLH^2 as a function of the dimensionless width W/H (β = 42.0°) and of the angle β (W/H = 2.6) at various pressures and different cell heights, respectively. Solid orange lines indicate our nonlinear theoretical prediction (Eq. 4). (G) Contour map of the dimensionless rotational stiffness as a function of W/H and β.

specimen. The theoretical prediction (see the supplementary materials) is plotted in continuous lines and matches precisely the force-displacement curves measured experimentally. For a given applied pressure P, the effective Young modulus E_c of a single cell is inferred from the linear response of the cell for small displacement and is expected to follow

$$E_c = \tan\theta_0 \frac{\cos\theta_0 + \theta_0\sin\theta_0}{\sin\theta_0 - \theta_0\cos\theta_0} P \quad (3)$$

where the initial spanned angle θ_0 obeys $\theta_0/\cos\theta_0 = W/H$ (see the supplementary materials). The comparison of the normalized modulus E_c/P as a function of the aspect ratio W/H is in excellent agreement with the theoretical prediction, confirming that the modulus only depends on the applied pressure and the geometry of the cell (Fig. 3C). Conversely, for large extension, the stiffness of the cell (Fig. 3B) tends toward the stretching stiffness of the pair of fabric laid flat, $E_{max} = 2E_f t/H$ (where E_f and t are the Young modulus and thickness of the fabric sheet, respectively), which is independent of pressure.

The angular stiffness of a nonsymmetric cell (β ≠ 0°) is obtained by measuring the torque M as a function of the applied deflection angle γ (Fig. 3, D and E). The effective angular stiffness K_r of the cell (linearized response; see the supplementary materials) is predicted to obey

$$\frac{K_r}{PLH^2} = \frac{W}{H}\frac{\cos\left(\theta_0 + \beta - \frac{\gamma_0}{2}\right) + 2\theta_0\sin\left(\theta_0 + \beta - \frac{\gamma_0}{2}\right)}{4\theta_0^2\cos\beta} \quad (4)$$

where $\theta_0 = \frac{W}{H}\frac{(2\beta-\gamma_0)\cos\beta}{2\sin\beta}$ is the initial value of spanned angle of arc W, L is the length of cell, and the initial folding angle γ_0 follows Eq. 1.

These predictions (continuous line in Fig. 3F) were confirmed by direct experimental measurements of the angular stiffness (with no adjustable parameter). Different configurations (e.g., points 1 and 2 in the contour map in Fig. 3G) are expected to display different actuated geometries but similar structural stiffness for the same pressure. Overall, we found that the mechanical stiffness of an isolated Gaussian cell is directly proportional to its internal pressure, whereas its activated geometry is independent of pressure, suggesting the possibility of tuning the stiffness independently of the shape (for a general discussion of the stiffness of the shell structure as a function of the spatial periodicity of the cells, see the supplementary materials).

Assembling Gaussian cells into programmable structures

We now explore how elementary folding and contraction mechanisms of individual cells can be used to program shape morphing of plates into complex structures. The induced curvature can be discretized as $\kappa = \gamma/\ell$, where ℓ is the spacial periodicity of the cells' distribution (Fig. 2A). Developable surfaces such as generalized cylinders or cones are readily obtained by controlling the deflection angle

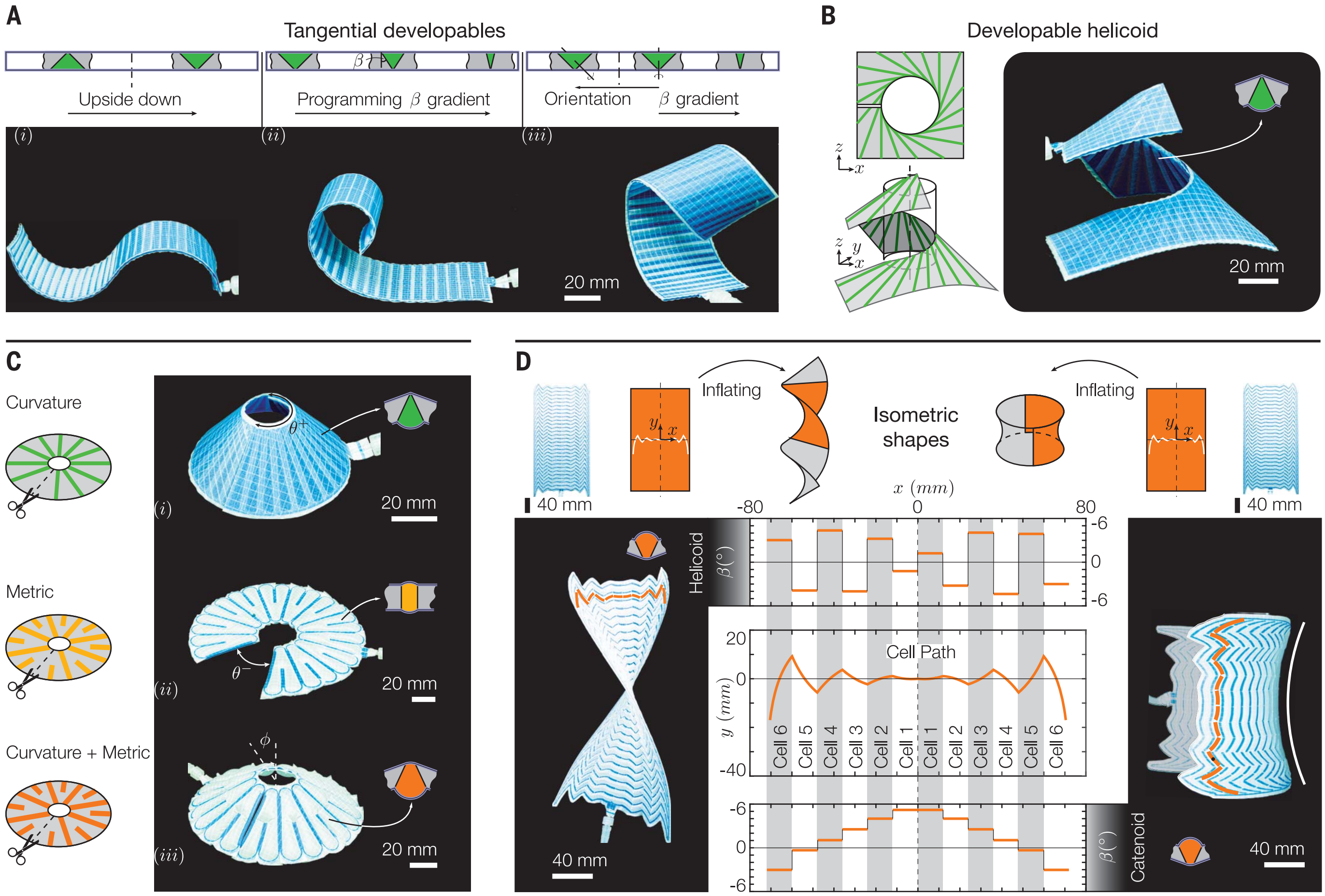

Fig. 4. Programming bending and Gaussian curvatures in multicellular structures. (**A**) Developable shapes based on triangular cells (see movie S2): (i) an "S" shape with opposite curvatures (ii) a spiral with a linearly increasing curvature, and (iii) a curling shape with variable curvature direction. (**B**) Developable helicoid with generating lines tangent to the central circle (see movie S2). (**C**) A sectioned annulus with radial cells can morph into (i) a truncated cone with angular surplus (pure bending with triangular cells), (ii) a flat annulus sector with angular deficit (metric change with rectangular cells), or (iii) a perfect truncated cone when bending and metric changes are programmed simultaneously (see movie S3). (**D**) Selection between isometries (see movie S4). The same metric change (programmed zigzag pattern) leads to degenerated isometric shapes from helicoid to catenoid. Controlling local bending breaks the degeneracy (for a discussion of inverse programming, see the supplementary materials).

locally. Figure 4A illustrates different examples in which the sign of a constant curvature is alternated by piece, the amplitude of the curvature is proportional to the curvilinear abscissa, or the direction of the bending direction is modified, leading, respectively, to (i) an "S" shape, (ii) a spiral with linearly increasing curvature, or (iii) a curly ribbon (see movie S2). A developable helicoid is finally obtained by selecting the director lines tangent to a central circle cut inside the initially flat structure, with an additional transverse cut to allow for deployment (Fig. 4B and movie S2). Figure 4C and movie S3 demonstrate, with the simple example of a slit annulus morphing into a cone, why curvature and metric changes should be used simultaneously. Programming solely curvature without in-plane contraction on such a slit annulus does lead to a cone (Fig. 4Ci), but one with an overlap angle $\theta^+ = 2\pi(1 - \sin\varphi)$, where φ is the cone angle. Conversely, an annulus with cells solely programmed for in-plane contraction will remain flat when actuated with an angular deficit $\theta^- = 2\pi(1 - \lambda_{eff})$, where λ_{eff} is the effective contraction ratio at the scale of the whole structure (Fig. 4Cii). Only when both the active curvature and the in-plane contraction were combined in the programming did we observe that the annulus deployed into a perfect target conical shape (Fig. 4Ciii).

In-plane contraction dictates the Gaussian curvature of the deployed structures. However, targeting this quantity alone only restrains the resulting shape to a family of isometries (*12*). In practice, the observed realization relies on a minimization of the finite bending energy of actual structures, which tends to limit the design space to peculiar solutions among these families (*33*, *34*). Archetypal catenoids and helicoids, minimal surfaces commonly illustrated with soap films, present the same distribution of Gaussian curvature. Merely programming in-plane contraction using cells of rectangular cross-section is therefore not enough to select between configurations. However, adjusting the internal angle of the walls allows for the control of the bending curvature in the direction perpendicular to the cells' path. As a result, for two structures designed with similar cell outlines [the zigzag patterns provide biaxial contraction (*35*)], precise adjustment of the internal angle leads to the desired helicoid (of programmed handiness) or catenoid shapes (*36*) (Fig. 4D and movie S4; for a discussion of the detailed design of the cells, see the supplementary materials). Although Gaussian cells are capable of curvature in the direction

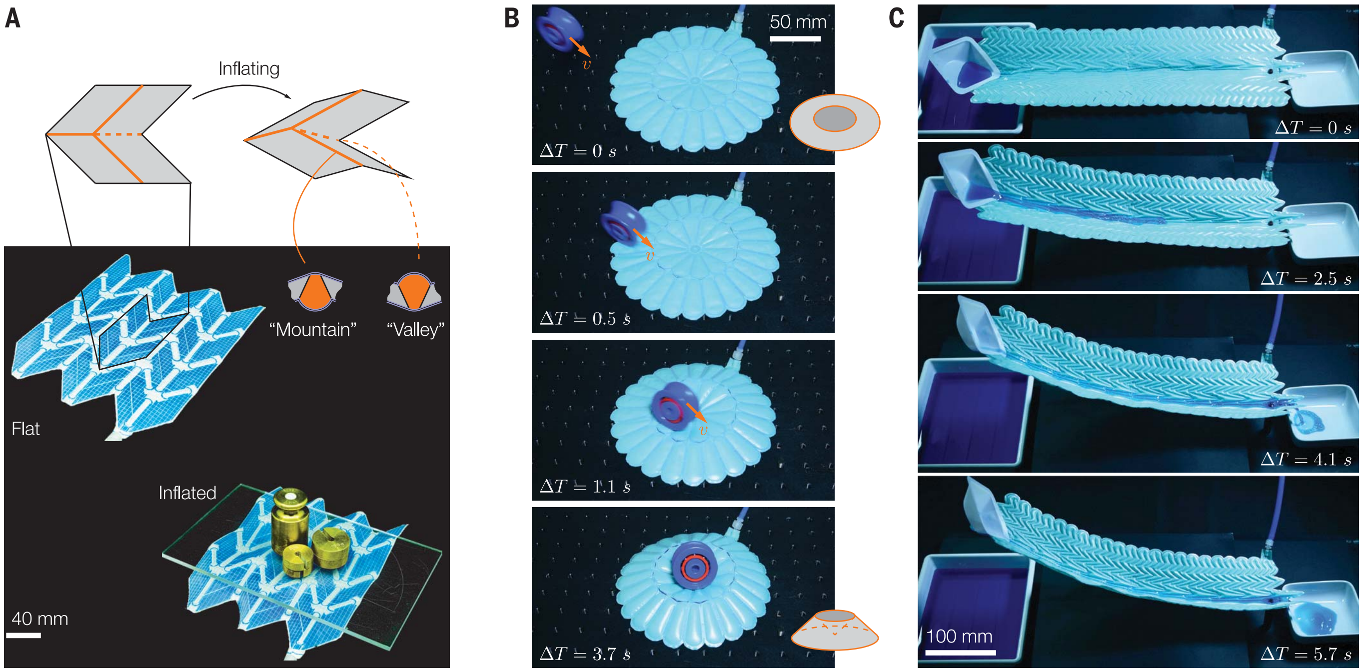

Fig. 5. Toward shape morphing robotics. (**A**) Self-actuated Miura-ori panel (see movie S5). Cells function as stiff "mountain" or "valley" creases (total load of 1 kg). (**B**) Volcano-shaped actuator (see movie S6). The initially flat disk is actuated in a fraction of second as a cylinder rolls over it at 10 cm/s. The cylinder (weight 40 g) remains trapped inside the deployed crater. (**C**) Upon inflation, a flat stripe bends into a doubly curved gutter track that permits manipulation and transport of liquids (see movie S7).

perpendicular to their axis, the use of alternating directions overcomes this constraint.

Much effort has been devoted recently to the design of origami structures (*25*, *26*); however, robust self-actuation remains an issue (*37*, *38*). Figure 5A presents a classical Miura-ori tessellation pattern (*39*) in which "mountain" and "valley" creases have been programmed using Gaussian cells. Upon inflation, the structure self-folds to the target configuration with a stiffness high enough to support a relatively heavy load (see movie S5). Beyond origami structures, their excellent stiffness, robustness to failure, and fast actuation suggest that pneumatic Gaussian cells are promising for applications in morphing robotics (for a discussion of performances and scalability, see the supplementary materials). Standard soft-robotics technologies generally rely on bending actuation of grabbing beam elements (*11*); however, robotic systems could be developed by harnessing the surface shape morphing achieved with Gaussian cells. Figure 5B illustrates an initially flat disk that adopts in a fraction of second the shape of a crater based on the cone transformation and traps an object rolling over (see movie S6, which also demonstrates how a ball can be guided by an active track). Although the presented examples are based on a single inlet and interconnected cells, more complex kinematics could be obtained by separating cells into subgroups that would be activated separately or by embedding mechanical valves between cells that could provide a sequential actuation (*40*, *41*). Finally, active surfaces may also be used to manipulate liquids. In Fig. 5C and movie S7, a long strip is programmed to morph into a curved gutter of positive Gaussian curvature (*35*) with a controlled bending direction, transferring liquid to a different container and demonstrating the versatile capabilities of the technique.

Toward shape-morphing robotics

Inspired by actuating cells observed in some plants, we have developed powerful and versatile Gaussian cells that provide stiff, fast, and reversible self-morphing of thin plates. Because metrics and curvature can be programmed simultaneously, these cells provide accurate control of the deployed geometry, imparting a high degree of mechanical stability to the resulting structure. Moreover, the stiffness of the deployed shell (proportional to applied pressure) can be tuned independently of its shape (dictated by the local configuration), opening up the possibility of developing large-scale morphing structures. Pneumatic Gaussian cells combine stiffness with a high level of control in shape programming, holding significant promise for applications in which avoiding mechanical instabilities is crucial, but also for haptic devices in which both shape and stiffness controls are valuable output information for the end user. Made using standard 3D printing techniques with consumer-grade materials, the resulting robust, shape-changing surfaces bring the concept of material-machine closer to providing a large-scale and general commodity product.

REFERENCES AND NOTES

1. H. Liang, L. Mahadevan, *Proc. Natl. Acad. Sci. U.S.A.* **108**, 5516–5521 (2011).
2. X. Cheng, Y. Zhang, *Adv. Mater.* **31**, e1901895 (2019).
3. L. Hines, K. Petersen, G. Z. Lum, M. Sitti, *Adv. Mater.* **29**, 1603483 (2017).
4. T. J. Jones, E. Jambon-Puillet, J. Marthelot, P.-T. Brun, *Nature* **599**, 229–233 (2021).
5. R. F. Shepherd *et al.*, *Proc. Natl. Acad. Sci. U.S.A.* **108**, 20400–20403 (2011).
6. J. Wang, D. Gao, P. S. Lee, *Adv. Mater.* **33**, e2003088 (2021).
7. M. Li, A. Pal, A. Aghakhani, A. Pena-Francesch, M. Sitti, *Nat. Rev. Mater.* **7**, 235–249 (2022).
8. Y. Yang, K. Vella, D. P. Holmes, *Sci. Robot.* **6**, eabd6426 (2021).
9. W. Kim *et al.*, *Sci. Robot.* **4**, eaay3493 (2019).
10. D. Melancon, B. Gorissen, C. J. García-Mora, C. Hoberman, K. Bertoldi, *Nature* **592**, 545–550 (2021).
11. B. Gorissen *et al.*, *Adv. Mater.* **29**, 1604977 (2017).
12. D. J. Struik, *Lectures on Classical Differential Geometry* (Addison-Wesley Press, 1950).
13. J. Dervaux, M. Ben Amar, *Phys. Rev. Lett.* **101**, 068101 (2008).
14. A. B. Rebocho, P. Southam, J. R. Kennaway, J. A. Bangham, E. Coen, *eLife* **6**, e20156 (2017).
15. Y. Klein, E. Efrati, E. Sharon, *Science* **315**, 1116–1120 (2007).
16. E. Efrati, E. Sharon, R. Kupferman, *Phys. Rev. E Stat. Nonlin. Soft Matter Phys.* **80**, 016602 (2009).
17. J. Kim, J. A. Hanna, M. Byun, C. D. Santangelo, R. C. Hayward, *Science* **335**, 1201–1205 (2012).
18. A. Nojoomi, J. Jeon, K. Yum, *Nat. Commun.* **12**, 603 (2021).
19. H. Aharoni, Y. Xia, X. Zhang, R. D. Kamien, S. Yang, *Proc. Natl. Acad. Sci. U.S.A.* **115**, 7206–7211 (2018).
20. T. van Manen, S. Janbaz, A. A. Zadpoor, *Mater. Horiz.* **4**, 1064–1069 (2017).
21. J. Gu *et al.*, "Geodesy: Self-rising 2.5D tiles by printing along 2D geodesic closed path," in *Proceedings of the 2019 CHI Conference on Human Factors in Computing Systems* (ACM, 2019), pp. 1–10.

22. J. H. Pikul *et al.*, *Science* **358**, 210–214 (2017).
23. E. Siéfert, E. Reyssat, J. Bico, B. Roman, *Nat. Mater.* **18**, 24–28 (2019).
24. E. Siéfert, E. Reyssat, J. Bico, B. Roman, *Soft Matter* **16**, 7898–7903 (2020).
25. L. H. Dudte, E. Vouga, T. Tachi, L. Mahadevan, *Nat. Mater.* **15**, 583–588 (2016).
26. S. J. Callens, A. A. Zadpoor, *Mater. Today* **21**, 241–264 (2018).
27. G. P. T. Choi, L. H. Dudte, L. Mahadevan, *Nat. Mater.* **18**, 999–1004 (2019).
28. A. S. Gladman, E. A. Matsumoto, R. G. Nuzzo, L. Mahadevan, J. A. Lewis, *Nat. Mater.* **15**, 413–418 (2016).
29. J. W. Boley *et al.*, *Proc. Natl. Acad. Sci. U.S.A.* **116**, 20856–20862 (2019).
30. S.-J. Jeon, R. C. Hayward, *Soft Matter* **16**, 688–694 (2020).
31. S. Matschi *et al.*, *Plant Direct* **4**, e00282 (2020).
32. A. Mader, M. Langer, J. Knippers, O. Speck, *J. R. Soc. Interface* **17**, 20200358 (2020).
33. E. Efrati, E. Sharon, R. Kupferman, *J. Mech. Phys. Solids* **57**, 762–775 (2009).
34. S. Armon, E. Efrati, R. Kupferman, E. Sharon, *Science* **333**, 1726–1730 (2011).
35. T. Gao, E. Siéfert, A. DeSimone, B. Roman, *Adv. Mater.* **32**, e2004515 (2020).
36. H. Aharoni, E. Sharon, R. Kupferman, *Phys. Rev. Lett.* **113**, 257801 (2014).
37. C. D. Santangelo, *Annu. Rev. Condens. Matter Phys.* **8**, 165–183 (2017).
38. S. Wu, T. Chen, H. Tsai, *J. Mech.* **35**, 627–639 (2019).
39. M. Schenk, S. D. Guest, *Proc. Natl. Acad. Sci. U.S.A.* **110**, 3276–3281 (2013).
40. L. Jin, A. E. Forte, K. Bertoldi, *Adv. Sci. (Weinh.)* **8**, e2101941 (2021).
41. L. C. van Laake, J. de Vries, S. M. Kani, J. T. Overvelde, *Matter* **5**, 2898–2917 (2022).
42. S. D. Guest, S. Pellegrino, "Inextensional wrapping of flat membranes," in *Proceedings of the First International Seminar on Structural Morphology*, R. Motro, T. Wester, Eds. (University of Montpellier, 1992), vol. 25, pp. 203–215.
43. D. Webb *et al.*, "Starshade mechanical architecture technology effort," paper presented at the 3rd AIAA Spacecraft Structures Conference, San Diego, CA, 4–8 January 2016.

ACKNOWLEDGMENTS

We thank H. Aharoni, E. Reyssat, and A. DeSimone for stimulating discussions and B. Moulia for botanical inspiration. **Funding:** This work was partly supported by the French ANR SecondSkin project (grant ANR-21-CE33-0018). **Author contributions:** T.G., J.B., and B.R. conceived and developed the pneumatic Gaussian cell concept. T.G., J.B., and B.R. conducted the experiments and analyzed the data. T.G., J.B., and B.R. developed the theoretical model. All authors wrote the manuscript. **Competing interests:** The authors declare no competing interests. **Data and materials availability:** All data are available in the main text or supplementary materials.

SUPPLEMENTARY MATERIALS

science.org/doi/10.1126/science.adi2997
Materials and Methods
Supplementary Text
Figs. S1 to S20
References
Movies S1 to S7

Submitted 17 April 2023; accepted 20 July 2023
10.1126/science.adi2997

Pneumatic cells toward absolute Gaussian morphing

Tian Gao, Jos Bico, and Benot Roman

Science, **381** (6660), .
DOI: 10.1126/science.adi2997

Editor's summary
Transforming a flat sheet into a curved object or vice versa usually leads to distortions such as wrinkles or cuts unless the Gaussian curvature is conserved, such as when turning a piece of paper into a cylinder or a cone. Drawing inspiration from bulliform cells in plants, which are believed to control the curvature in leaves to regulate water loss, Gao *et al*. designed thin panels with inflatable pneumatic cells that allow for pure in-plane or bending or combinations of the two. Thus, the authors were able to transform a flat surface into a shape with a different Gaussian curvature, with implications for the designs of soft robotics. —Marc S. Lavine